AIRFLOW MODEL TESTING TO DETERMINE THE DISTRIBUTION OF HOT GAS FLOW AND O/F RATIO ACROSS THE SPACE SHUTTLE MAIN ENGINE MAIN INJECTOR ASSEMBLY

L. Mahorter, J. Chik, D. McDaniels, and C. Dill
National Aeronautics and Space Administration
Marshall Space Flight Center, Alabama

ABSTRACT

Engine 0209, the certification engine for the new Phase II+ Hot Gas Manifold (HGM), showed severe deterioration of the Main Combustion Chamber (MCC) liner during hot fire tests. One theory on the cause of the damage held that uneven local distribution of the fuel rich hot gas flow through the main injector assembly was producing regions of high oxidizer/fuel (O/F) ratio near the wall of the MCC liner.

Airflow testing was proposed to measure the local hot gas flow rates through individual injector elements. The airflow tests were conducted at the Marshall Space Flight Center's Air Flow Dual Leg Facility using full-scale, geometrically correct models of both the current Phase II and the new Phase II+ HGMs. Different main injector flow shield configurations were tested for each HGM to ascertain their effect on the pressure levels and distribution of hot gas flow. Instrumentation located on the primary faceplate of the main injector measured hot gas flow through selected injector elements. These data were combined with information from the current space shuttle main engine (SSME) power balances to produce maps of pressure, hot gas flow rate, and O/F ratio near the main injector primary plate. O/F distributions were compared for the different injector and HGM configurations.

INTRODUCTION

This series of tests was initiated when unusually severe deterioration of the MCC liner developed during hot fire testing of the certification engine for the new Phase II+ Hot Gas Manifold design. Damage to the MCC included severe cracking on both the fuel and oxidizer sides, wall blanching, and baffle erosion. The goal of the airflow tests was to evaluate uneven local O/F ratios as a potential cause of damage to the MCC liner by deriving and comparing the local hot gas flow rates through the main injector elements of both the Phase II and Phase II+ HGMs. Indications of potentially damaging O/F ratios would be large differences in O/F distributions or O/F ratios above stoichiometric (8) which could provide free oxygen to react with the chamber wall.

FACILITY DESCRIPTION

The airflow tests were conducted at MSFC's Airflow Facility (Dual Leg) in building 4777 (north addition). Flow into the fuel and oxidizer legs is individually controlled by valves which regulate the downstream model inlet pressure to a specified value, usually 1.72×10^6 N/m^2 (250 psi). Back pressure in the model is maintained by an exit valve located downstream of the model MCC. For this series of tests, the exit valve operated with an open area of .0124 sq. m. (19.2 sq. in.). These conditions allow approximately 30 kg/sec (66.3 lbm/sec) of mass flow through the model. The inlet pressures are adjusted to produce a flow split of 71% of total mass flow on the fuel side and 29% on the oxidizer side. At these conditions, the facility is capable of providing steady state flow for at least 15 seconds.

Data acquisition equipment in the facility includes a Pressure Systems, Inc. (PSI) system and a Hewlett-Packard (HP) computer, as well as various other measurement devices. The PSI system has individually calibrated transducers for every model pressure measurement. Facility and data measurements are manipulated and stored by the HP computer, then sent from the HP to the VAX 6310.

MODEL DESCRIPTIONS

Both the Phase II and the Phase II+ test HGMs are modular, full-scale, aluminum models. Major differences between the Phase II and Phase II+ designs are: the change from three to two fuel transfer ducts (FTD) with a larger total flow area, an increase in the fuel turn-around duct (TAD) cross-sectional area, a larger fuel bowl volume, a larger injector bowl volume, and more efficient, aerodynamically rounded duct inlets and outlets. The interior contours of the models match those of the engine designs from before the turbine inlets to the MCC. Figure 1 shows the Phase II and Phase II+ injector bowl geometry.

Both models have turbine simulators on the fuel and oxidizer sides. The turbine simulators consist of a porous plate to produce a pressure drop and swirl vanes to simulate turbine exit swirl conditions at Full Power Level (FPL or 109%).

The same main injector is used by both models. The injector is actual flight hardware modified for use with the airflow models. Interchangeable flow shields can be configured to produce a variety of flow

shield configurations. Figure 2 shows a schematic of the flow through the main injector elements. Due to the design of the model, neither the LOX flow through the LOX posts nor the hydrogen coolant flow in the interpropellant plate region are simulated.

INSTRUMENTATION

Both models use similar instrumentation. For these tests the instrumentation was concentrated at the turbine exit and in the main injector region. Turbine exit pressure taps are located just downstream of the turbine simulator swirl vanes on the hub wall, eight on the fuel side and twelve on the oxidizer side. These measurements were used to calculate the turbine exit conditions.

In the injector region, some special instrumentation was developed specifically for these tests. Plugs, Fig. 3, were used in some locations to replace the primary faceplate nut. The plugs measured the MCC pressure at the injector primary plate and the stagnated hot gas pressure of a non-flowing element.

The basic instrumentation in the injector region is the same although the Phase II and Phase II+ models use different injector bowls and flow shield configurations. The injector outer racetrack has pressure taps and instrumentation plugs located on three circumferential planes. The injector itself has eighty-five pressure taps in various locations. Twenty-four of these pressure taps are located on the upper face-plate of the injector, while the others are located on the front and back of the flow shields. The pressure taps on the flow shields are mainly located at the center height of the shields but some are located closer to the secondary injector plate and some closer to the LOX dome. Most of the instrumented shields are grouped near the fuel transfer ducts or near the oxidizer transfer ducts.

TEST PLAN

All testing was done with inlet line pressures of approximately 1.72×10^6 N/m^2 (250 psi) and 109% power level swirl vanes in the turbine simulator. In all, five engine configurations were tested: 1. Phase II HGM with Phase II flow shields; 2. Phase II HGM with no flow shields; 3. Phase II+ HGM with Phase II+ flow shields; 4. Phase II+ HGM with Phase II flow shields; and 5. Phase II+ HGM with no flow shields. For each engine configuration, injector element plugs were located in at least 100 locations. In order to minimize disturbance of the flow, no more than 20 injector element plugs were installed in a well distributed pattern at any given time.

DATA REDUCTION

For every run, the facility data acquisition system collected and stored seven frames of data per label. Each frame consisted of the mean of ten measurements made by the PSI system. After verification of test conditions, all seven frames were transferred to the VAX, where they were put into the database.

FACILITY CALCULATIONS

The mass flows through the fuel and oxidizer legs, $\dot{M}_f$ and $\dot{M}_x$ respectively, were calculated at the facility from the following equations:

$$\dot{M}_f = 1.098\, C_f\, A_f \sqrt{\frac{(PTF)(\Delta P)}{T_f}} \qquad C_f = .99,\ A_f = .0559\ m^2\ (86.59\ in^2)$$

$$\dot{M}_x = 1.098\, C_x\, A_x \sqrt{\frac{(PTX)(\Delta P_x)}{T_x}} \qquad C_x = .99,\ A_x = .0285\ m^2\ (44.18\ in^2)$$

NON-DIMENSIONALIZATION

The pressure data was non-dimensionalized and scaled to engine conditions using a coefficient of pressure, C_p, linked to the fuel turbine exit conditions. The mean of the steady-state data frames was calculated for each measurement of each run. Fuel turbine exit static pressure, P_{fte}, was calculated from the mean of the turbine exit hub wall statics. The mean turbine exit pressure was then used to calculate 1-dimensional turbine exit dynamic pressure, q_{fte}.

$$C_p = \frac{P - P_{fte}}{q_{fte}} \qquad q_{fte} = C_{fte} \frac{\dot{M}_f^2\, T_f}{P_{fte}}$$

For plug data, a $C_{\Delta p}$ was calculated from the difference between the MCC pressure and the hot gas pressure, both measured by the primary plate plug, divided by q_{fte}.

CALCULATION O/F RATIO FROM PLUG DATA

The pressure drop across the injector element is scaled to engine conditions by:

$$\Delta P_{scaled} = C_{\Delta p} * Q_{te\ engine}$$

An inlet velocity for the retainer holes can be calculated and used to calculate the mass flow of hot gas through the injector element.

$$u = \sqrt{\frac{\Delta P_{scaled}}{\frac{1}{2}\rho_{hot\ gas} K}} \qquad \dot{m}_{hot\ gas} = u * \rho_{hot\ gas} * A$$

The hot gas mass flow is then divided into hydrogen and oxygen mass flows.

$$\dot{m}_{fuel\ in\ hg} = \frac{\dot{m}_{hot\ gas}}{1 + \left(\frac{O}{F}\right)_{hot\ gas}}$$

The amount of hydrogen and oxygen in the hot gas is dependent on the origin of the hot gas, since the fuel and oxidizer preburners have different mixture ratios, $(O/F)_{hot\ gas}$. The flow split between the two sides is shown in Fig. 5.

A final O/F ratio for that element is then calculated to include the oxygen flow from the LOX dome, $\dot{m}_{LOX}$, and the hydrogen coolant flow through the secondary plate into the hot gas, $\dot{m}_{coolant}$. The theoretical distribution of LOX flow by injector row is: .967% of total LOX flow for each element of rows 1 and 2; .974% on row 3; 1.006% on rows 4, 7 and 8; and .998 on rows 8 through 13.

$$\left(\frac{O}{F}\right)_{element} = \frac{\dot{m}_{LOX} + \dot{m}_{ox\ in\ hg}}{\dot{m}_{fuel\ in\ hg} + \dot{m}_{coolant}}$$

The scaling factors used, table I, were taken from the 109% power level conditions in the Phase II+ power balance 86A, ref. 1 and the Phase II power balance, ref. 2.

Table I. Power Balance Data Used

	Phase II	Phase II+
$Q_{te\ engine}$	5.64×10^5 N/m^2 (81.82 psia)	5.61×10^5 N/m^2 (81.4 psia)
$\rho_{hot\ gas}$	12.10 kg/m^3 (.7554 lbm/ft^3)	12.17 kg/m^3 (.7597 lbm/ft^3)
$\dot{m}_{coolant}$	1.93 kg/sec (4.26 lbm/sec)	1.89 kg/sec (4.33 lbm/sec)
$\dot{m}_{LOX}$	.6545 kg/sec (1.443 lbm/sec)	.6559 kg/sec (1.446 lbm/sec)
$(O/F)_{hot\ gas}$	.8006	.7872
mean $(O/F)_{element}$	6.45	6.45
w/ out secondary plate coolant:		
$(O/F)_{hot\ gas}$	.8269	.8135
$(O/F)_{hg}$ (fuel side)	.8789	.8599
$(O/F)_{hg}$ (ox. side)	.7108	.7101
mean $(O/F)_{element}$	6.67	6.67

RESULTS

Most injector plug data was collected on rows 13, 12, 11, 9, 7, 5, 3, and 1. Figure 5 shows the O/F ratios for these rows for the Phase II HGM with Phase II flow shields configuration. The drop in O/F ratio occurring between 130° and 230° is due to the low O/F ratio of the hot gas coming from the oxidizer preburner. The O/F ratios on rows 1 through 12 are grouped with a spread of approximately .5 O/F ratio, while row 13 has a lower O/F ratio than these inner rows. This O/F ratio distribution is typical of all of the configurations, but the model configurations with no flow shields on the injector tend to have a slightly more uniform O/F ratio distribution. For all configurations the O/F ratios are less than 7.2.

CONFIGURATION COMPARISONS

Baseline Configurations Figure 6 shows the comparison between the Phase II baseline configuration (Phase II HGM with Phase II flow shields) and the Phase II+ baseline configuration (Phase II+ HGM with Phase II+ flow shields) on row 13. On this row, the Phase II+ configuration generally has slightly higher O/F ratios than the Phase II configuration. Exceptions are mainly in the regions near 0° to 30° and 330° to 360°, where differences in fuel side transfer ducts are greatest. On the oxidizer side, the Phase II+ shows O/F ratios that are generally .3 O/F higher. Figure 7 shows the same comparison for row 12. On this row the two configurations are very similar, although there is still a difference of approximately .2 O/F on the oxidizer sides. This oxidizer side difference in O/F is almost nonexistent by row 11. The difference between the two configurations are generally small on all of the inner rows.

Phase II+ HGM Configurations Figures 8 and 9 show comparisons of rows 12 and 13 for the three different flow shields configurations tested on the Phase II+ HGM. On both rows, the no flow shields condition has a higher O/F ratio, although the difference is smaller on row 12. On rows 11 and 9 the O/F ratios are comparable, while the no flow shields condition produces slightly lower O/F ratios on rows 7 through 1. Comparisons of the Phase II+ HGM shielded configurations show very little difference in the O/F ratios produced by the Phase II+ and the Phase II shield configurations.

Phase II HGM Configurations Figures 10 compares the two Phase II HGM configurations with the Phase II flow shields and with no flow shields for row 13. The no flow shields condition for the Phase II+ and the Phase II HGMs show very similar trends with higher O/F ratios on the outer rows, comparable O/F ratios in the middle rows, and lower O/F ratios in the inner rows.

RADIAL DISTRIBUTIONS

Figures 11 and 12 show the radial O/F ratio distributions at 356° and 140°. The difference in overall O/F level between the two plots is due to the differences in fuel and oxidizer side O/F ratios. The elements on the 356° radial receive their flow from the fuel side preburner, while those on the 140° radial receive theirs from the oxidizer side. Row 13 has the lowest O/F ratio, with the O/F ratio generally rising from row 12 to row 7. The drop in O/F ratio shown in rows 1 through 3 is due to the lower mass flow of LOX through these elements.

CONCLUSIONS

For all of the configurations row 13 had the lowest O/F ratio, usually below the mean injector value of 6.45. If it were desired to further lower the row 13 O/F ratio there is no obvious flow shield configuration which would produce these results, since the shieldless injector configurations produce higher O/F ratios on row 13.

Since all configurations tested showed a maximum O/F ratio of less than 7.2 and the differences between the Phase II and the Phase II+ baseline configurations were small, it is unlikely that the differences in O/F ratio caused by hot gas flow are the primary cause of MCC wall deterioration in Engine 0209. It is possible, however, that the hot gas distribution may be contributing to deterioration caused by another source.

REF: 1. IL 88-05-019, Rocketdyne, "SSME Phase II+ Performance Prediction - Power Balance Model Version SSME86A", Process Date May 4, 1988.
2. OL 87RC09038, Rocketdyne, "SSME Phase 2 Predicted Engine Performance", Process Date April 27, 1987. Phase II Power Balance.

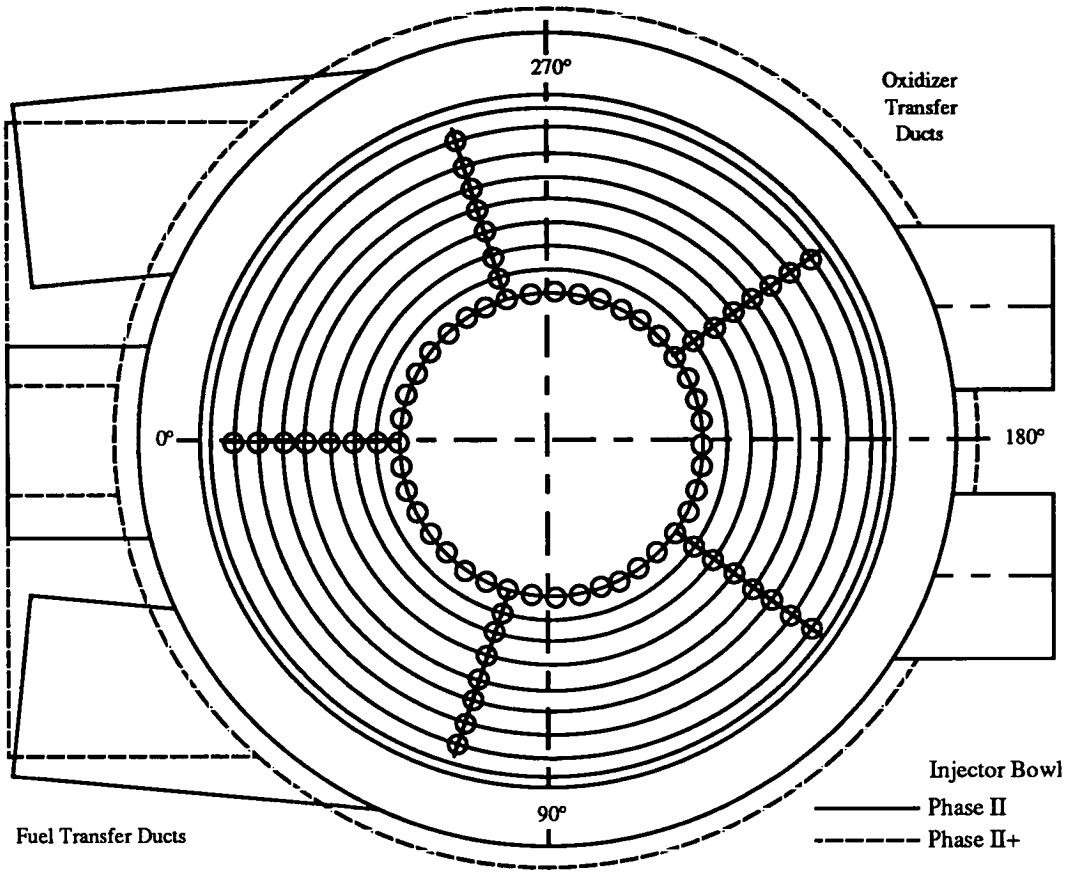

Figure 1. Schematic of Main Injector Bowls
(view from MCC towards LOX dome)

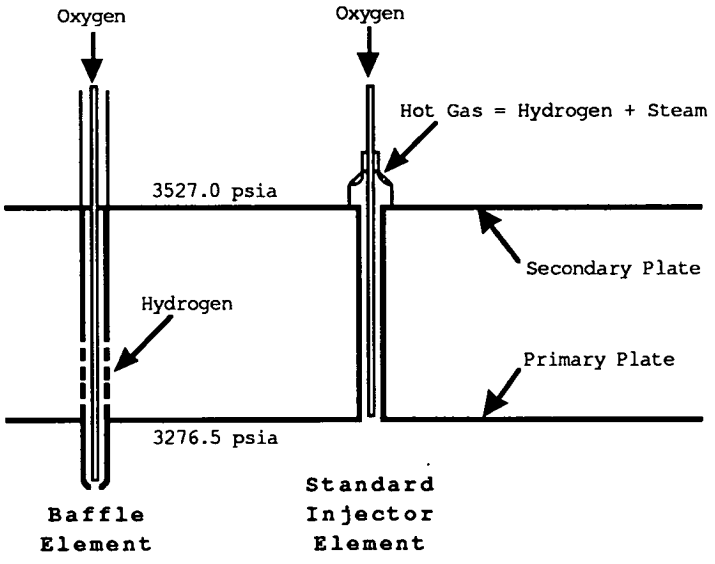

Figure 2. Schematic of Main Injector Element Flows

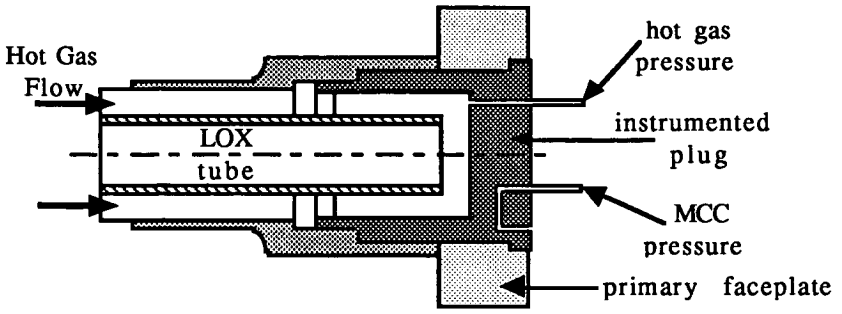

Figure 3. Instrumentation Plug for Primary Face Plate Nut

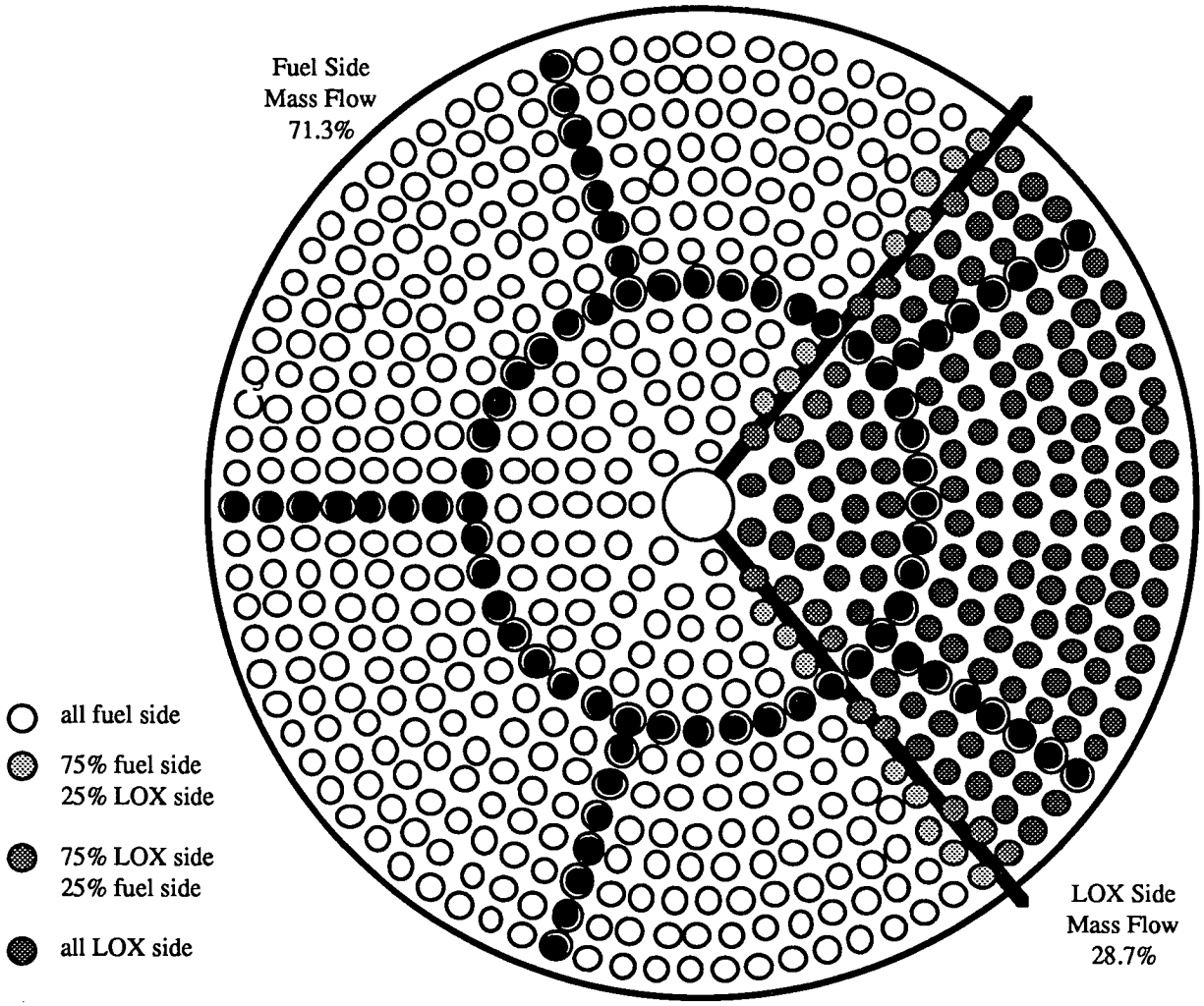

Figure 4. Fuel to Oxidizer Side Flow Split

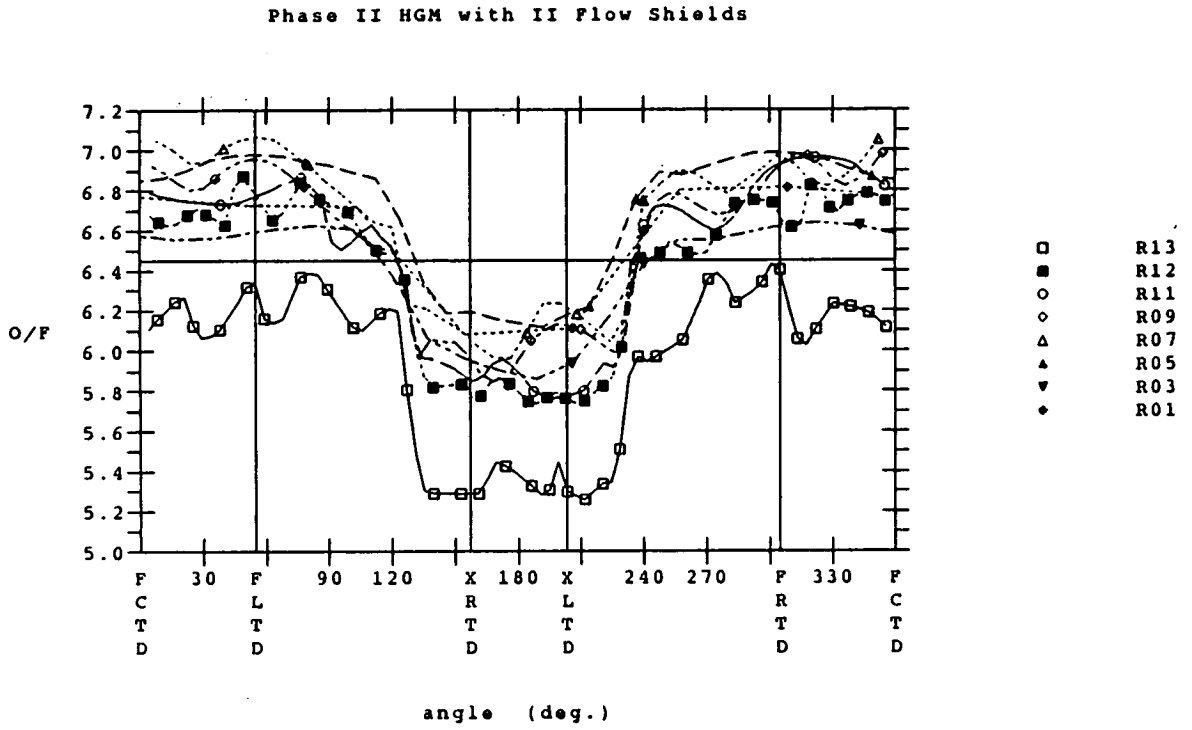

Figure 5. Phase II HGM with Phase II Flow Shields

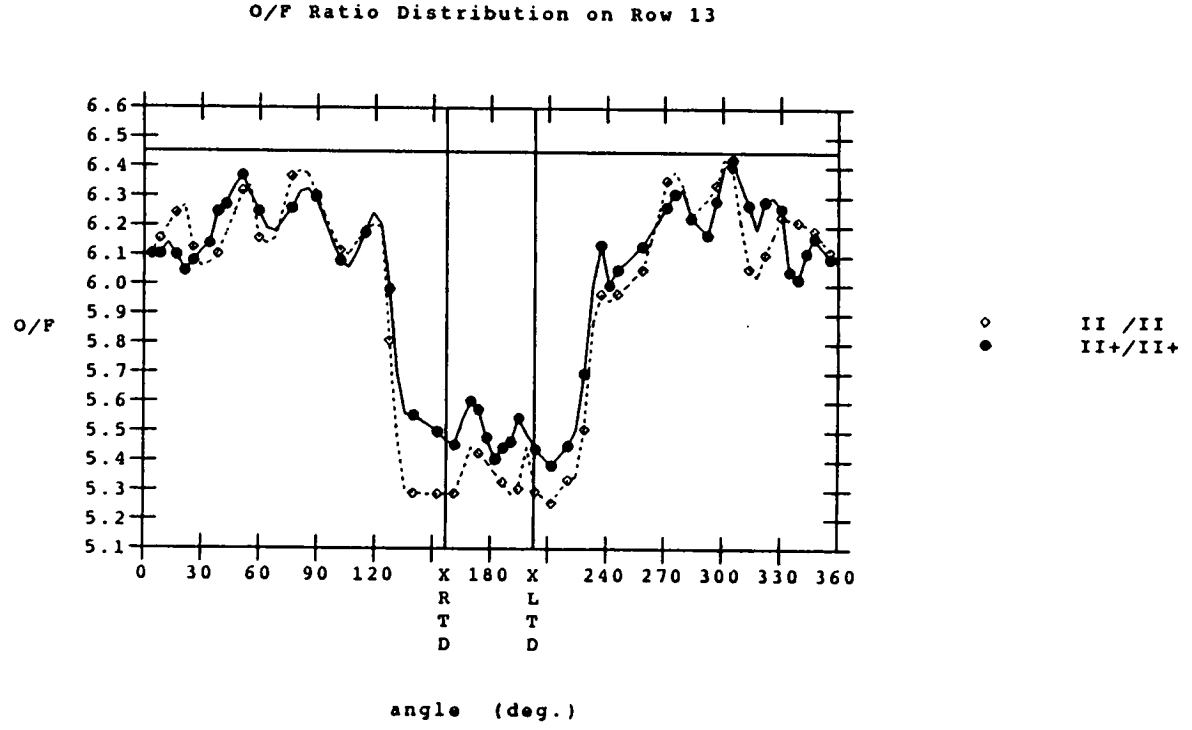

Figure 6. Comparison of Baseline Configurations
Row 13

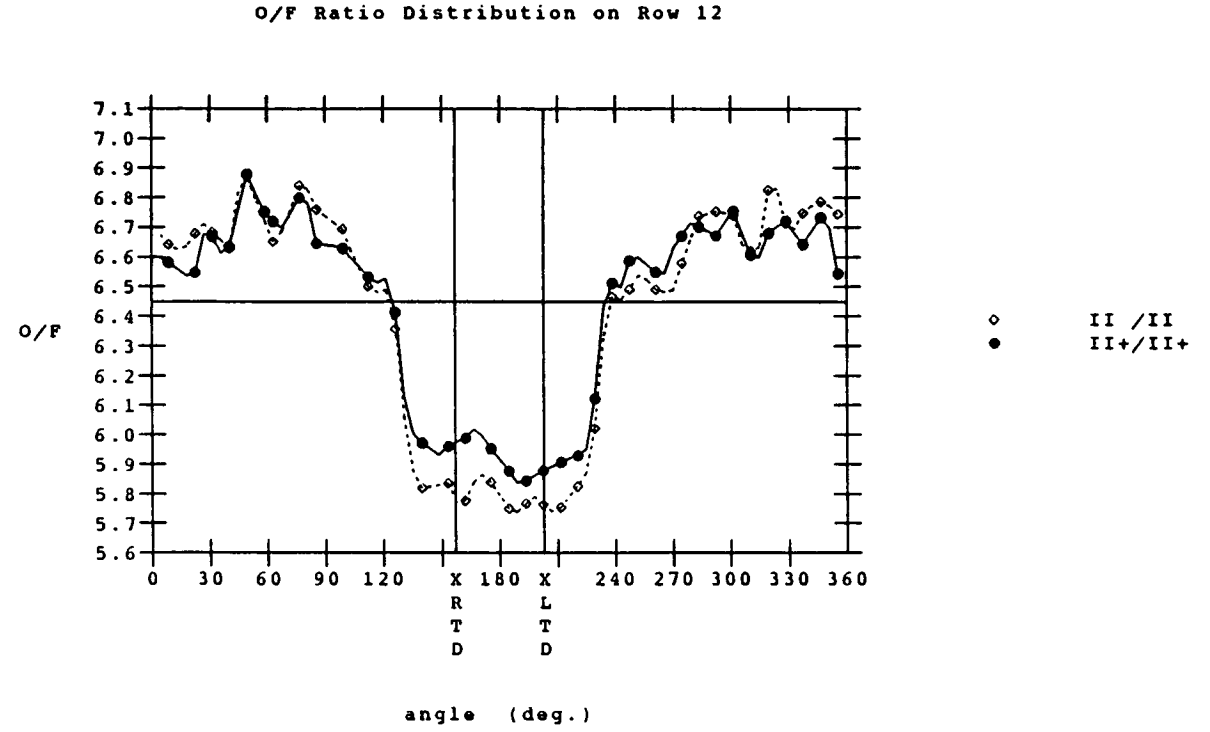

Figure 7. Comparison of Baseline Configurations
Row 12

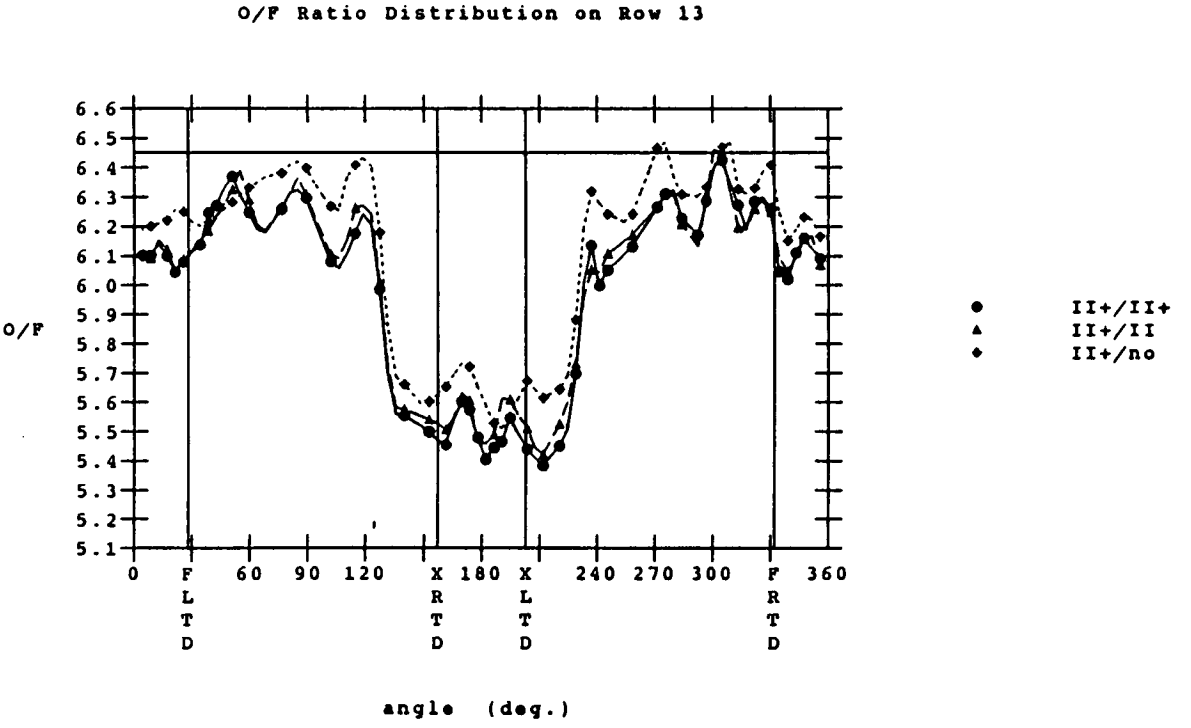

Figure 8. Comparison of Phase II+ HGM Configurations
Row 13

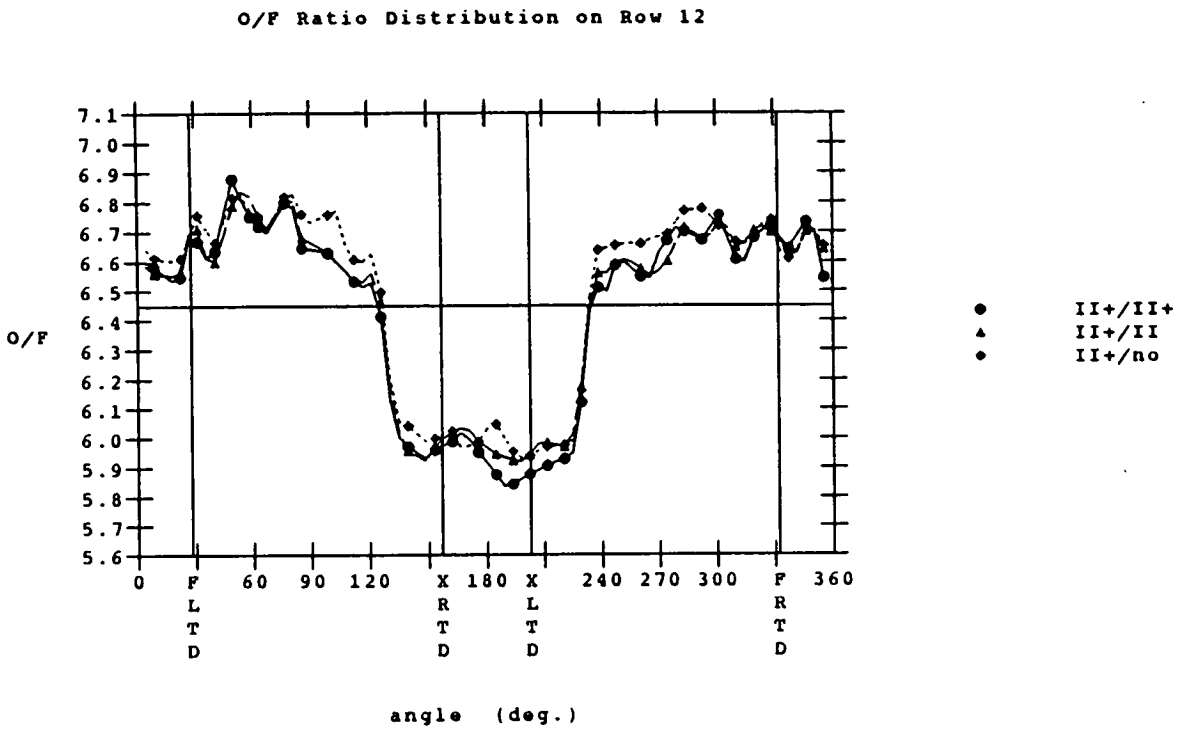

Figure 9. Comparison of Phase II+ HGM Configurations
Row 12

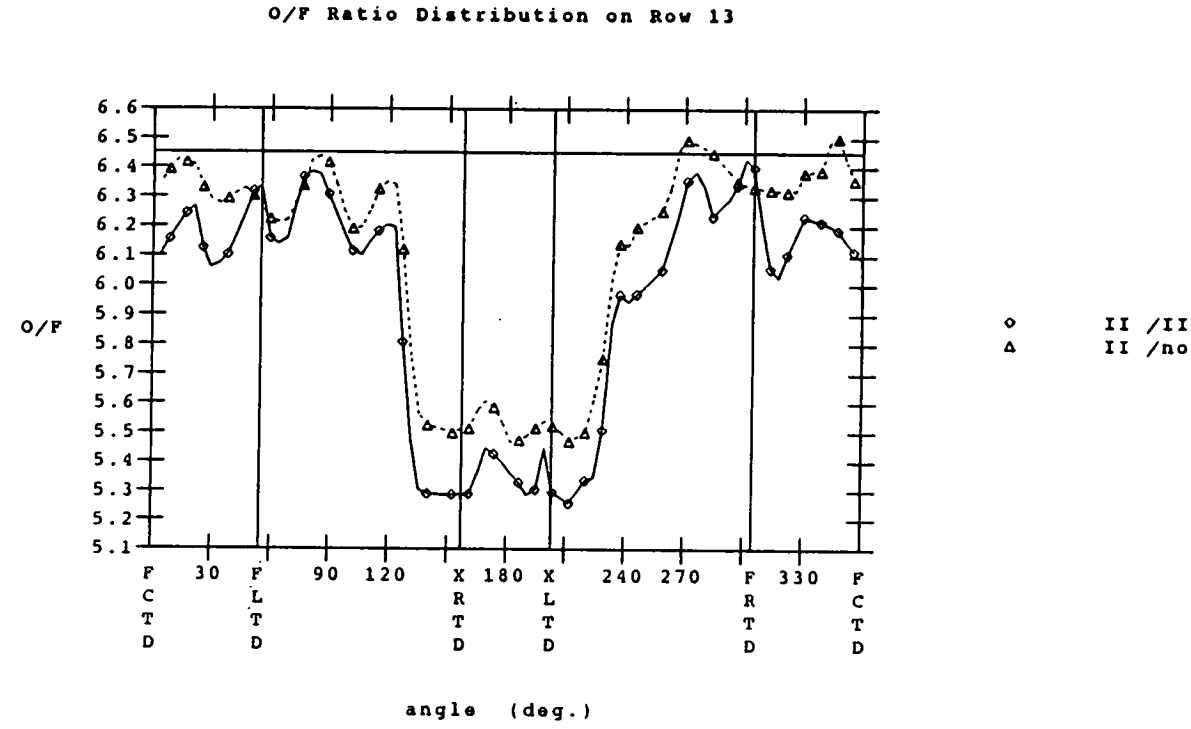

Figure 10. Comparison of Phase II HGM Configurations
Row 13

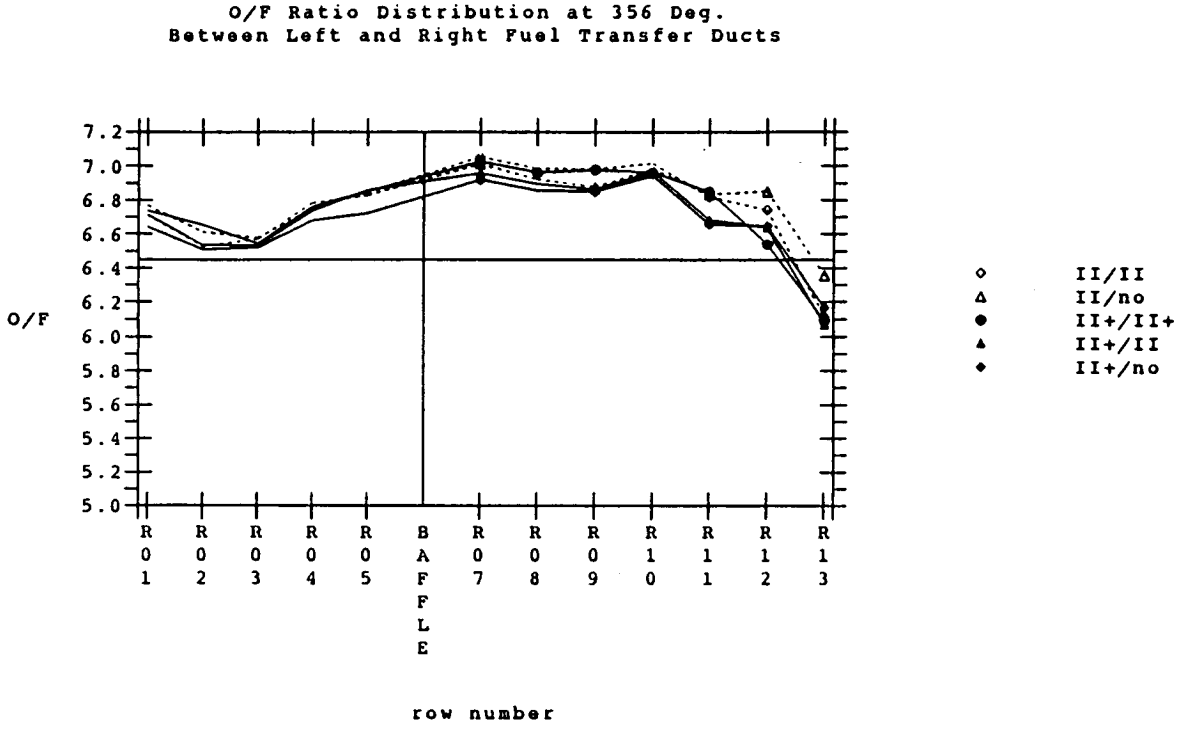

Figure 11. Radial O/F Ratio Distribution at 356 Deg.

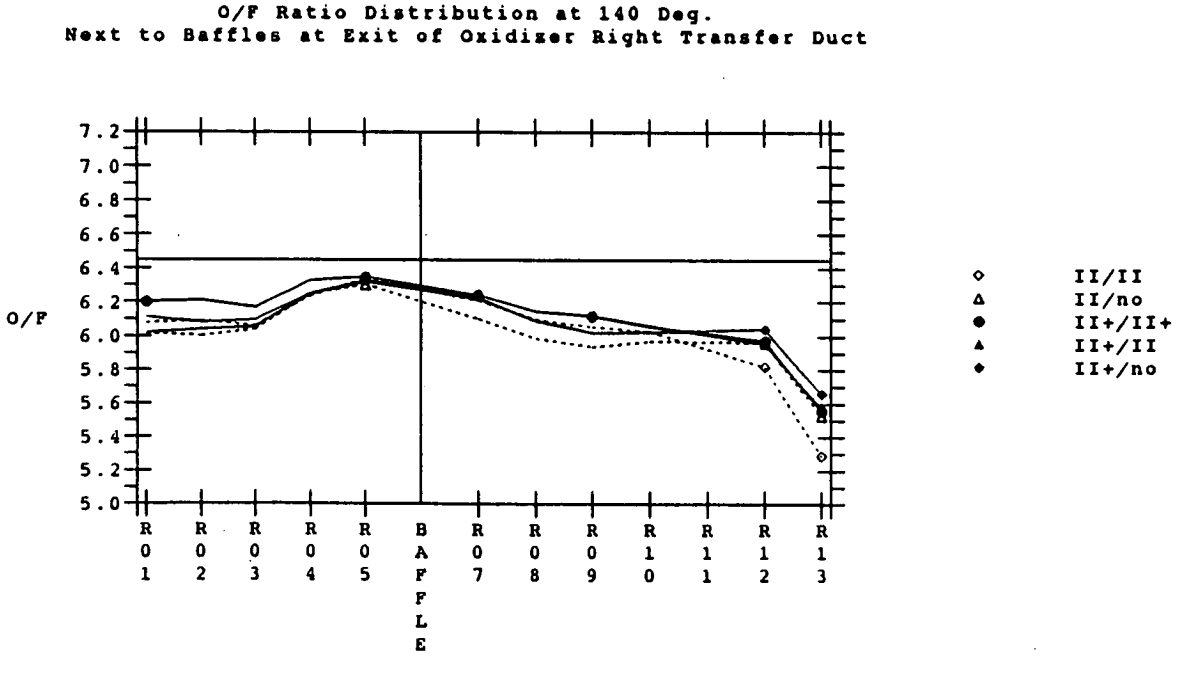

Figure 12. Radial O/F Ratio Distribution at 140 Deg.